

Electronic Supplementary Information

A Self-assembly Route to Porous Polyaniline/Reduced Graphene Oxide Composite Materials with Molecular-level Uniformity for High-performance Supercapacitors

Jifeng Wu, ^{ac} Qin'e Zhang, ^a Jingjing Wang, ^a Xiaoping Huang, ^a and Hua Bai^{ab}*

a. Address here. College of Materials, Xiamen University, Xiamen, 361005, China, P.R.

Email: baihua@xmu.edu.cn

b. Graphene Industry and Engineering Research Institute, Xiamen University, Xiamen, 361005, China, P.R.

c. Department of Physics, Fudan University, Shanghai, 200433, China, P. R.; Institute of Natural Sciences, Westlake Institute for Advanced Study, Westlake University, Hangzhou 310064, China, P. R.

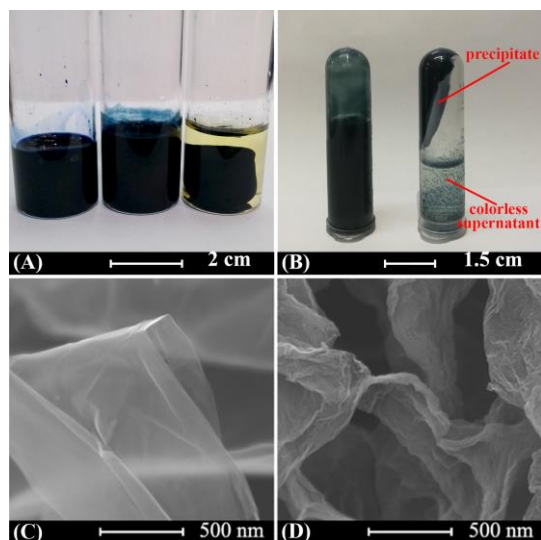


Fig. S1 (A) Left: photograph of polyaniline dissolved in NMP; middle: photograph of PANI@GO in water/NMP blend solvent; right: photograph of gel obtained by treating the blend solution with ascorbic acid at 90 °C for 2 hours. (B) The PANI PANI@GO blend solution before (left) and after (right) centrifuged at 3000 rpm for 10 min. (C) SEM of GO sheets. (D) SEM of PANI@GO sheets.

There is no precipitate forming after PANI solution was centrifuged at 3000 rpm for 10 min, because PANI chains are well dispersed in NMP. When these chains absorb on GO sheets, they can be removed from the solution brought by GO sheets by centrifugation. The colorless supernatant indicates that all the PANI chains have assembled onto GO sheets and precipitate during centrifugation.

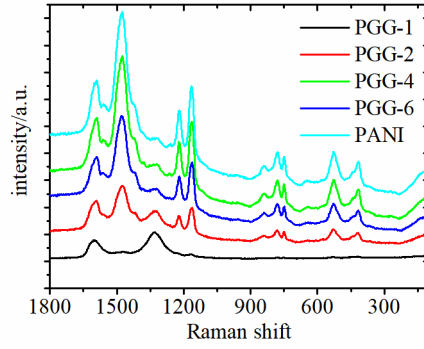


Fig. S2 Raman spectra of PGG-1, PGG-2, PGG-4, PGG-6 and PANI.

The interaction between graphene and PANI film was investigated using Raman spectrum analysis. As shown in **Fig. S2**, the Raman spectrum of PGG-4 shows two distinctive peaks centered at 1359 and 1586 cm^{-1} that correspond to D and G bands of graphene, respectively. The bands located at 1174 cm^{-1} (C-H), 1220 cm^{-1} (C-N) and 1348 cm^{-1} (C-N⁺) illustrates the presence of PANI in the PGG-4 hybrid.^[1]

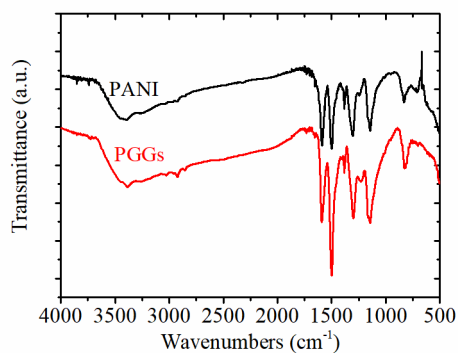


Fig. S3 FTIR spectra of PGGs composite.

FT-IR measurement was carried out to characterize the chemical structure of the GPHs hybrid. As shown in **Fig. S3**, several characteristic peaks associated with the amide group were observed. The main peaks at 1592 and 1499 cm⁻¹ can be assigned to the stretching vibrations of quinone and benzene rings, respectively. The band at 1300 cm⁻¹ corresponds to the C–N stretching vibration. The in-plane bending of C–H is reflected in the 1144 cm cm⁻¹ peak. The peak at 828 cm⁻¹ is attributed to the out-of-plane bending of C–H. All of the above peaks show that PANI exists in PGG.

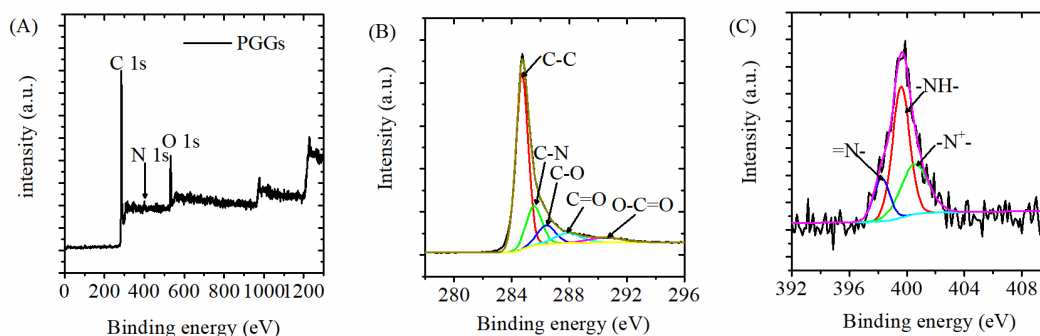


Fig. S4 XPS spectrum of PGGs; (A), (B) XPS data of the C 1s and N 1s regions of the PGGs, respectively.

XPS was also used to characterize the sample in a wide scan (**Fig. S4**). **Fig. S4** (A) shows the composition of the obtained PGGs (C, N and O). Further studies on the high-resolution XPS of the N 1s region indicates that there are three different electronic states: the benzenoid amine with binding energy (BE) centered at 399.6 eV, the quinoid amine with BE at 398.25 eV, and the nitrogen cationic radical ($-N^{+-}$) with BE at 400.54 eV, as shown in **Fig. S5** (C). **Fig. S4** (B) shows the of C 1s line, which is decomposed into five peaks with their BE of 284.7 (C–C), 285.6 (C–N), 286.55 (C–O), 288.03 (C=O), and 290.55 (O–C=O). The small C–O component indicates that GO was reduced successfully.

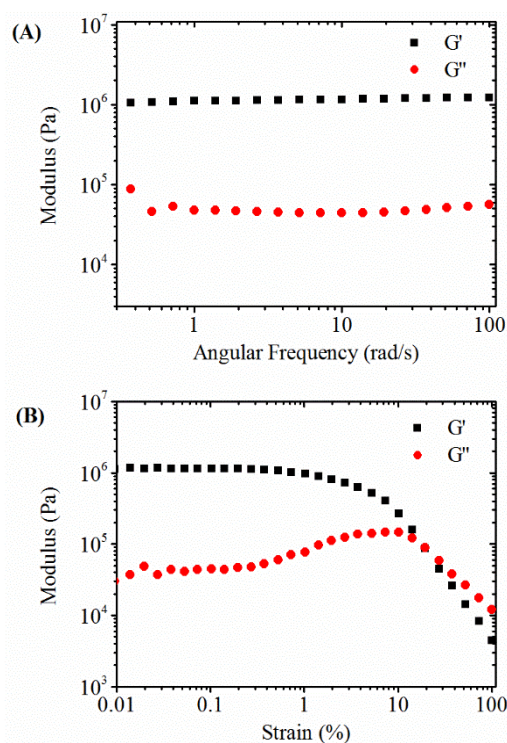


Fig. S5 (A) Plots of storage and loss moduli of PGG monoliths versus angular frequency. (B) Storage and loss moduli of PGG monoliths at different strains.

The PGG monoliths show typical gel rheological behaviour. The storage moduli (G') of the gel are frequency independent, and are much larger than the corresponding loss moduli (G''), indicating that elastic response of the PGG monoliths is predominant, and the composite is a strong hydrogel. The good mechanical properties allow the composite to be tailored into designed shape, and directly used as electrodes in supercapacitor devices without any additive. **Fig. S5 B** demonstrates the storage and loss moduli of PGG monoliths at different strains. The storage modulus dwindled with the increase of strain. However, at strain $>20\%$, the storage modulus became smaller than the corresponding loss modulus, indicating the hydrogel was damaged.

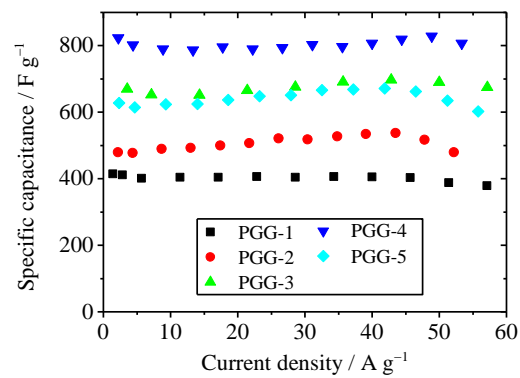


Fig. S6 Specific capacitances of PGGs with different PANI feeding ratio.

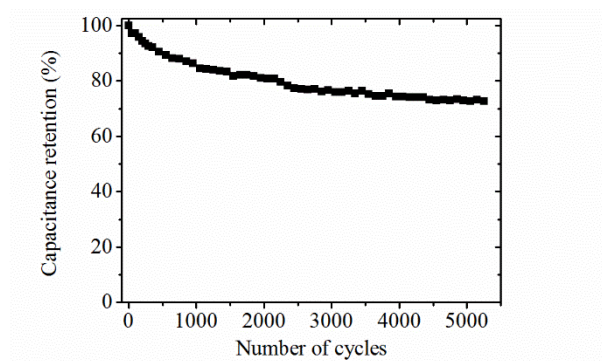


Fig. S7 Cycling stability of the PGGs electrode at a current density of 26.6 A g^{-1} (0-0.8V).

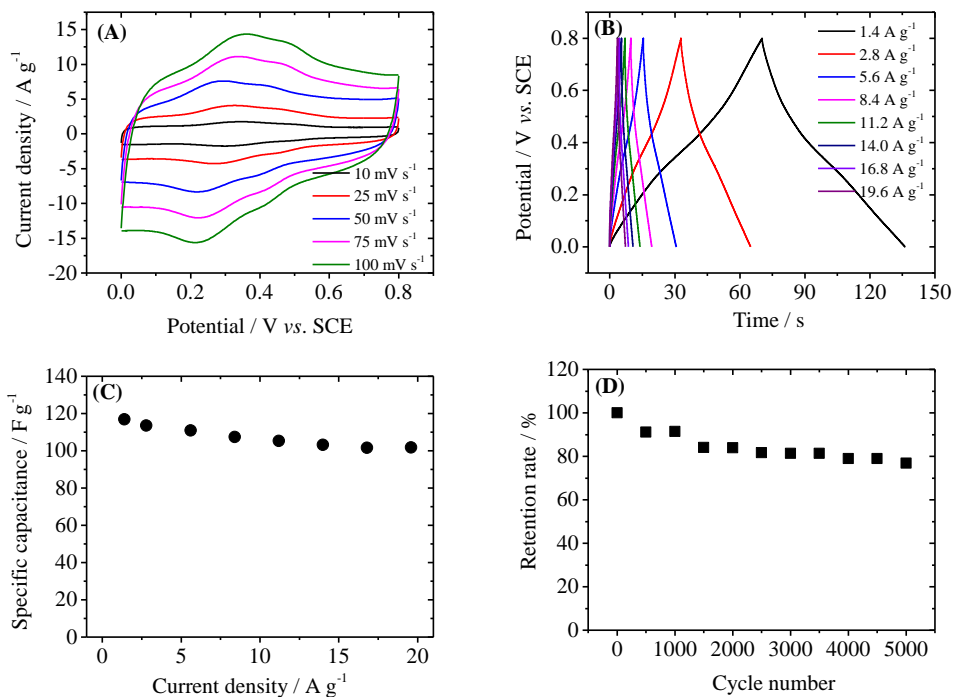


Fig. S8. Capacitive performance of PGG-4 tested in symmetric two-electrode devices (mass loading of both electrode: 2 mg cm⁻²). (A) CV curves of the device. (B) GCD curves of the device at the different current density. (C) Specific capacitances of the device versus current densities. (D) Cycling stability of the device at a current density of 16.8 A g⁻¹ (0 ~ 0.8V).

The specific capacitances of the device were calculated according to the following equation:

$$C_s = \frac{Jt}{\Delta V - IR}, \quad (1)$$

and $J = \frac{I}{m}, \quad (2)$

where ΔV is the highest voltage of the device during charge process, and m is the total mass of the two electrodes; I is the current applied on the device, t is the discharge time, and IR represents the voltage drop at the beginning of the discharge process, caused by internal

resistance of the system. To calculate average specific capacitance of single electrode and compare it with three-electrode data, a factor of 4 should be multiplied to C_s in Equation 1.

The average specific capacitance of single electrode is 467.2 F g^{-1} at 2.8 A g^{-1} , lower than the value measured in three electrode system. In fact, the two-electrode test was performed on a symmetric device, with PGG-4 composite as both the anode and cathode. When works as cathode, PGG-4 has relatively small specific capacitance, because in negative potential range ($< 0 \text{ V vs. SCE}$), PANI does not has electrochemical activity. As a result, the specific capacitance of symmetric two-electrode device is smaller than that measured in three-electrode system.

Table S1. Comparison of the capacitances based on PANI/RGO composite. ^a

Materials	Current density (mA/cm ²)	Specific capacitance (F/g)	Electrolyte	Cycling stability	Mass loading (mg/cm ²)	Ref
Highly Ordered Polyaniline Nanorods on Reduced Graphene Oxide Patterns	22	757	1M Na ₂ SO ₄ (0V-1 V)	1700 cycles 90%	0.55	[2]
Flexible graphene–polyaniline composite paper	7.6	490	1M H ₂ SO ₄ (-0.2V-0.8 V)	1000 cycles 80% 5 A/g	0.76	[3]
Phase-Separated Polyaniline/Graphene Composite	305.7	783	1M H ₂ SO ₄ (0V-0.8V)	10000 cycles 81.1% 16.7 A/g (0V-0.8V)	11.2	[4]
Biotemplated hierarchical polyaniline composite electrodes	8.8	452	1M H ₂ SO ₄ (0V-0.6V)	1000 cycles 87% 1 A/g (0V-0.6V)	2.2	[5]
Layered polyaniline/graphene film	14.2	192	1M H ₂ SO ₄ (-0.2 V-0.8V)	1000 cycles 84% 2 A/g	1.42	[6]
Hierarchical graphene oxide/polyaniline nanocomposites	214	657	PVA–H ₂ SO ₄ (0V-0.8V)	1000 cycles 91.1%	10.7	[7]
Conductive Polymer Hydrogels	40	700	1M H ₂ SO ₄ (0V-0.8V)	1000 cycles 90%	2	[8]
Hydrothermal synthesis of nanostructured graphene/polyaniline composites	17.5	233	1M H ₂ SO ₄ (-0.2V-0.8V)	1000 cycles 75% 50 mV/s	1.75	[9]
Vertically Aligned Tunable Polyaniline on Graphene/ZrO ₂ Nanocomposites	2.8	675	1M H ₂ SO ₄ (0V-0.8V)	1000 cycles 92%	1.4	[10]
graphene wrapped polyaniline nanofibers	21	655	1M H ₂ SO ₄ (-0.2V-0.8V)	1000 cycles 85% 10 A/g	2.1	[11]

Metal-Free Supercapacitor Electrode Material	38	360	1M H ₂ SO ₄ (0V-0.8V)		3.8	[12]
3D Polyaniline Porous Layer Anchored Pillared Graphene Sheets	60	423	0.5M H ₂ SO ₄ (0V-0.8V)	4000 cycles 90%	3	[13]
Aniline Tetramer-Graphene Oxide Composites	39.6	584	1M H ₂ SO ₄ (0V-0.8V)	2000 cycles 100%	0.66	[14]
Free-standing three-dimensional graphene and polyaniline nanowire arrays hybrid foams	9.5	598	1M H ₂ SO ₄ (0V-0.8V)	5000 cycles 80% 1 A/g	0.95	[15]
3D Polyaniline Architecture by Concurrent Inorganic and Organic Acid Doping	60	350	1M H ₂ SO ₄ (0V-0.7V)	500 cycles 90%	1-1.5	[16]
Three-Dimensional Graphene Frameworks	90	538	1M H ₂ SO ₄ (0V-1V)		9	[17]
Porous nitrogen and phosphorus co-doped carbon nanofiber networks	100	168	6M KOH (-1V-0V)	10000 cycles 94%	5	[18]
graphene hydrogel films as a substrate: the importance of nano-architecturing	106	530	1M H ₂ SO ₄ (-0.1V-0.9V)	10000 cycles 93% 100 A/ g	1.06	[19]
Polyaniline/Reduced Graphene Oxide Composite Electrode	377.4	808	1M H ₂ SO ₄ (0V-0.8V)	1000 cycles 73%	7.1	This work

^a All the specific capacitance data were measured in a three-electrode system.

References

1. M. Cochet, G. Louarn, S. Quillard, J. P. Buisson, S. Lefrant, *J. Raman Spectrosc.*, 2000, **31**, 1041.
2. M. Xue, F. Li, J. Zhu, H. Song, M. Zhang, T. Cao, *Adv. Funct. Mater.*, 2012, **22**, 1284.
3. H. Cong, X. Ren, P. Wang, S. Yu, *Energy Environ. Sci.*, 2013, **6**, 1185.
4. J. Wu, Q. Zhang, A. Zhou, Z. Huang, H. Bai, L. Li, *Adv. Mater.*, 2016, **28**, 10211.
5. C. Chang, Z. Hu, T. Lee, Y. Huang, W. Ji, W. Liu, J. Yeh, Y. Wei, *J. Mater. Chem. A*, 2016, **4**, 9133.
6. Z. Tong, Y. Yang, J. Wang, J. Zhao, B. Su, Y. Li, *J. Mater. Chem. A*, 2014, **2**, 4642.
7. D. Li, Y. Li, Y. Feng, W. Hu, W. Feng, *J. Mater. Chem. A*, 2015, **3**, 2135.
8. W. Li, H. Lu, N. Zhang, M. Ma, *ACS Appl. Mater. Interfaces*, 2017, **9**, 20142.
9. R. Wang, M. Han, Q. Zhao, Z. Ren, X. Guo, C. Xu, N. Hu, L. Lu, *Sci. Rep.*, 2017, **7**, 44562.
10. S. Giri, D. Ghosh, C. Das, *Adv. Funct. Mater.*, 2014, **24**, 1312.
11. N. Hu, L. Zhang, C. Yang, J. Zhao, Z. Yang, H. Wei, H. Liao, Z. Feng, A. Fisher, Y. Zhang, Z. Xu, *Sci. Rep.*, 2016, **6**, 19777.
12. Y. Xu, Y. Tao, X. Zheng, H. Ma, J. Luo, F. Kang, Q. Yang, *Adv. Mater.*, 2015, **27**, 8082.
13. P. Sekar, B. Anothumakkool, S. Kurungot, *ACS Appl. Mater. Interfaces*, 2015, **7**, 7661.
14. J. Yan, L. Yang, M. Cui, X. Wang, K. Chee, N. Viet Cuong, V. Kumar, A. Sumboja, M. Wang, P. Lee, *Adv. Energy Mater.*, 2014, **4**, 1400781.
15. P. Yu, X. Zhao, Z. Huang, Y. Li, Q. Zhang, *J. Mater. Chem. A*, 2014, **2**, 14413.
16. Y. Gawli, A. Banerjee, D. Dhakras, M. Deo, D. Bulani, P. Wadgaonkar, M. Shelke, S. Ogale, *Sci. Rep.*, 2016, **6**, 21002.
17. M. Yu, Y. Huang, C. Li, Y. Zeng, W. Wang, Y. Li, P. Fang, X. Lu, Y. Tong, *Adv. Funct. Mater.*, 2015, **25**, 324.

18. G. Xu, B. Ding, J. Pan, J. Han, P. Nie, Y. Zhu, Q. Sheng, H. Dou, *J. Mater. Chem. A*, 2015, **3**, 23268.
19. Y. Wang, X. Yang, L. Qiu, D. Li, *Energy Environ. Sci.*, 2013, **6**, 477.